Catalysis Science & Technology

PAPER

View Article Online
View Journal | View Issue

Cite this: *Catal. Sci. Technol.*, 2018, **8**, 5091

Chemoselective reduction of heteroarenes with a reduced graphene oxide supported rhodium nanoparticle catalyst†

Alena Karakulina, Aswin Gopakumar, Zhaofu Fei and Paul J. Dyson *

Received 22nd May 2018,
Accepted 20th August 2018

DOI: 10.1039/c8cy01046c

rsc.li/catalysis

Rhodium nanoparticles immobilized on reduced graphene oxide were obtained from the microwave-induced thermal decomposition of $Rh_6(CO)_{16}$ in the ionic liquid [bmim][BF_4] (bmim = 1-butyl-3-methylimidazolium cation) in the absence of additional stabilizing agents. The resulting rhodium nanoparticles are <4 nm in diameter and are evenly dispersed on the reduced graphene oxide. The composite was evaluated as a catalyst for the chemoselective hydrogenation of quinoline and other heteroarenes containing N- and O-heteroatoms. A high selectivity for the heterocyclic ring was achieved, typically >99%, without interfering with other reducible groups, and with high conversions. Related catalysts prepared using conventional thermal heating were prepared for comparison purposes and were found to be considerably less active.

Introduction

The direct and selective hydrogenation of nitrogen containing aromatic compounds, particularly quinolines, remains a challenging reaction although numerous homogeneous and heterogeneous catalysts have been reported.[1,2] The development of novel heterogeneous systems able to operate under mild conditions is of significant interest despite their high vulnerability to poisoning by adsorbed hydrogenated quinoline intermediates. A range of heterogeneous catalysts, *i.e.* metal nanoparticles (NPs) supported on dendrimers,[3] metal oxides,[4,5] silica hollow nanospheres,[6] titania,[7] and mesoporous carbon nitride[8] have been evaluated in the hydrogenation of quinoline compounds.

Carbon materials with large specific surface areas are particularly attractive supports for nanoparticle catalysts, and, in the last decade, graphene has received special attention due to its two-dimensional structure and outstanding electronic and mechanical properties.[9] Graphene oxide possesses reactive oxygen-containing functional groups on the surface,[10] which enhance the polarity of the material, thus promoting its use in liquid-phase reactions. The oxygen-containing groups can act as nucleation sites that anchor metal ions to facilitate the dispersion of metal NPs.[11–13] Graphene-supported metal NP composite materials have been used as chemical sensors,[14,15] electrodes for fuel cells[16] and other energy-related devices,[17–19] and as catalysts for hydrogenation reactions[20] and transformations of bio-based substrates.[11,21]

The general route used to obtain metal NP–graphene composite materials involves the simultaneous reduction of metal salts adhered to or in proximity to the graphene oxide surface. Beller and co-workers reported the preparation of cobalt nanoparticles on a nitrogen-doped graphene and Al_2O_3 support and used the nanocomposite as a catalyst for the selective hydrogenation of heteroarenes.[22] Subsequently, they reported an iron–nitrogen-doped graphene/core–shell catalyst and applied it in the oxidative dehydrogenation of N-heterocycles.[23] The nanocomposite was obtained at high temperatures (up to 800 °C) and required ligands such as 1,10-phenanthroline. Rh NPs derived from $Rh(NO_3)_3$ and supported on rGO have been used to catalyze the hydroformylation of 1-hexene.[24]

Microwave induced thermal decomposition of metal precursors in ionic liquid (IL) media represents a promising variation of this approach,[25,26] as ILs efficiently absorb microwaves due to their high dielectric constants.[27,28] The microwave-assisted IL method combines the advantages of traditional microwave synthesis (fast and energy efficient) and IL solvents (microwave absorbers and structure-directing agents).[29] Metal carbonyl complexes are known to decompose under microwave heating in ILs yielding metal NPs with relatively small and uniform sizes.[30,31] Starting from $Rh_6(CO)_{16}$, the only side product is CO, no additional ligands are required and no salt by-products are formed. This approach has been used to prepare metal and metal oxide particles and biomass-based nanocomposites.[32,33]

Institut des Sciences et Ingénierie Chimiques, Ecole Polytechnique Fédérale de Lausanne (EPFL), CH-1015 Lausanne, Switzerland. E-mail: paul.dyson@epfl.ch

† Electronic supplementary information (ESI) available: Additional characterization details. See DOI: 10.1039/c8cy01046c

Herein, we describe the application of microwave induced thermal decomposition of a discrete hexarhodium cluster, $Rh_6(CO)_{16}$, in an ionic liquid to afford Rh NPs immobilized on reduced graphene oxide (rGO). The resulting composite material is an excellent catalyst for the selective reduction of quinolines and other heteroarenes.

Results and discussion

The rGO substrate was prepared using a literature method[34] (see the ESI†) and characterized by transmission electron microscopy (TEM) (Fig. S1, ESI†). The rGO sheets comprise large stacked sheets and possess typical corrugation/wrinkles, which are characteristic of this material.[35,36] The surface area of the rGO was determined by nitrogen adsorption, with the nitrogen adsorption–desorption isotherm corresponding to type IV and possessing a hysteresis loop[37] and a specific surface area of 470 $m^2\ g^{-1}$ (Fig. S2, ESI†). X-ray photoelectron spectroscopy (XPS) was used to determine the degree of reduction of the rGO sheets, revealing the presence of the expected type and abundance of surface groups (Fig. S3, ESI†).[38]

The rGO sheets and the hexanuclear carbonyl cluster, $Rh_6(CO)_{16}$, were dispersed in the IL [bmim][BF_4] (bmim = 1-butyl-3-methylimidazolium cation) without any stabilizing additives. Conventional thermal decomposition and microwave dielectric heating were applied to generate the Rh NP–rGO composites from the suspension as shown in Scheme 1.

TEM analysis shows that the Rh NP–rGO composite prepared using conventional thermal decomposition contains Rh NPs that are not uniformly dispersed on the rGO as well as free Rh NPs present in the suspension (Fig. S4, ESI†). The Rh NPs on the surface of the rGO sheets have a mean diameter of 20 nm (for the NPs on the surface of the reduced graphene oxide). The prolonged thermolysis of NP precursors in the presence of an IL and rGO has previously been shown to result in the formation of large metal particles,[33,39] and rapid microwave heating allows improved morphological control of NPs compared to conventional heating.[33,40] Thus, the $Rh_6(CO)_{16}$–rGO suspension in [bmim][BF_4] was irradiated with microwaves (20 W) for 6 minutes to afford Rh NPs of *ca.* <4 nm in diameter that adhere to the rGO surfaces (Fig. 1). The Rh NPs are dispersed over the rGO sheets although in some regions the density of the Rh NPs is high, but nonetheless they remain dispersed.

The Rh content in the Rh NP–rGO material was determined by atomic adsorption spectroscopy (AAS) after washing the suspension with water in order to remove the IL. The Rh content was found to be 18.31% (similar to that of the material obtained by conventional thermal decomposition, 22.14%) and in good agreement with the value of 19.6% obtained from XPS analysis (Fig. 2). XPS was also used to explore the surface oxidation state of the Rh NPs in the Rh NP–rGO composite prepared *via* microwave treatment (Fig. 2). The survey spectrum indicates the presence of Rh, C and O in the composite material (Fig. 2). The Rh 3d XPS spectrum contains two peaks corresponding to the Rh $3d_{5/2}$ and $3d_{3/2}$ states from spin–orbital splitting. Each peak was fitted using the doublets corresponding to zero-valent and oxidized rhodium. Rh $3d_{5/2}$ can be deconvoluted into two distinguishable peaks with different binding energies, *i.e.* 307.20 eV and 308.18 eV. The value of 307.20 eV of the curve-fitted Rh $3d_{5/2}$ component unambiguously corresponds to metallic Rh(0).[38,41] The other curve fitted to the deconvoluted Rh $3d_{5/2}$ peak is centered around 308.18 eV. Since the peaks in the region 307.6–309.6 eV are assigned to Rh(I), and the peaks between 308.8–311.3 eV are attributed to Rh(III),[24,42] the binding energy at 308.18 eV may correspond to rhodium in the Rh(I) and Rh(III) oxidation states.

A similar assignment applies to the Rh $3d_{3/2}$ peak. From the curve-fitting procedure, the fraction of rhodium oxide in the sample was estimated to be around 40%. The formation of an oxide layer on the surface of the Rh NPs is indirectly supported by the increase in the oxygen content after deposition of Rh NPs on the rGO surface. The oxygen content of the rGO sample, evaluated by XPS, was found to be 11.1% and increased to 26.1% in the Rh NP–rGO composite, presumably due to a surface oxide coating on the Rh NPs.[43,44] The powder X-ray diffraction (XRD) patterns of the Rh NP–rGO

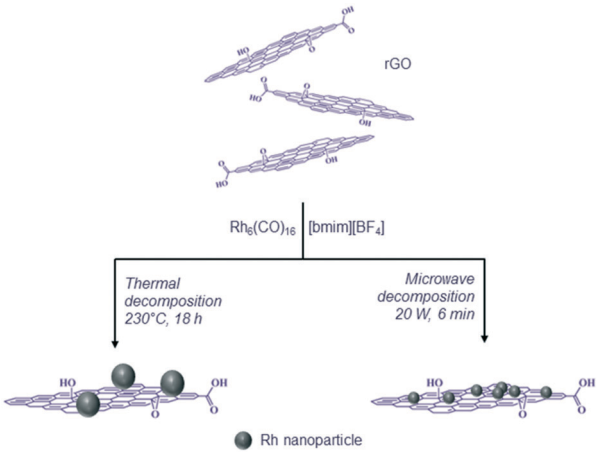

Scheme 1 Illustration of the route used to prepare the Rh NP–rGO composites applying conventional thermal and microwave dielectric heating methods.

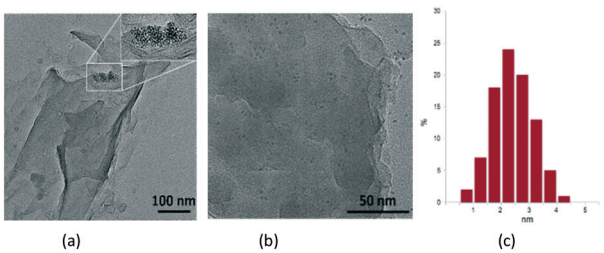

Fig. 1 TEM images of the Rh NP–rGO material comprising Rh NPs supported on rGO obtained by microwave heating (a) with the enlarged region showing a high-density region (inset of a) (b) and the corresponding Rh NP size distribution (c).

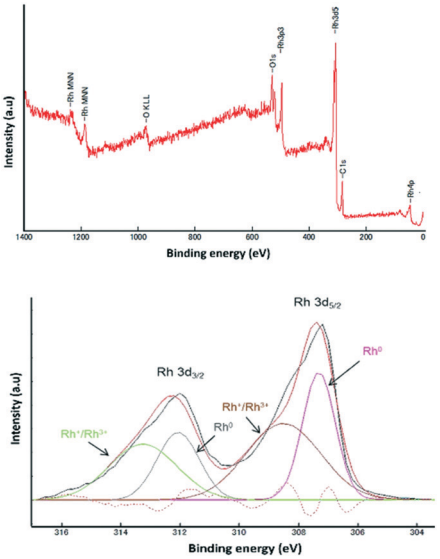

Fig. 2 XPS survey spectrum of the Rh NP–rGO composite obtained by microwave irradiation (top) and Rh 3d spectrum (bottom).

composite prepared *via* microwave treatment contain the characteristic reflections corresponding to the (111), (200), (220), (311) and (222) planes of crystals of metallic Rh (Fig. S5, ESI†).[45–47] The minor signals in the F 1s region at lower energy possibly correspond to the interactions of the anion in the IL with the Rh NP surface as described elsewhere.[48,49]

Evaluation of the catalytic activity of the Rh NP–rGO composite

The Rh NP–rGO composite, prepared using microwave dielectric heating, was re-dispersed in [bmim][BF_4] and evaluated as a catalyst in the hydrogenation of quinoline at a loading of 1 mol% (based on Rh). The selective reduction of the heteroaromatic ring of quinoline to afford 1,2,3,4-tetrahydroquinoline takes place in quantitative yield under 30 bar of H_2 at 80 °C (Table 1, entry 1). By extending the reaction time, 1,2,3,4-tetrahydroquinoline could be obtained quantitatively at a lower pressure of 10 bar H_2 (Table 1, entry 5). Note that the related composite prepared by thermal heating is less active, *i.e.* under the same conditions it affords the 1,2,3,4-tetrahydroquinoline product in 74% yield, albeit with equally high selectivity. The yield and selectivity achieved with the Rh NP–rGO catalyst are comparable with those of Rh NPs in Lewis acidic ionic liquids that are sensitive to moisture[50] and N-graphene-modified cobalt nanoparticles (Co_3O_4–Co/NGr@α-Al_2O_3)[22] which operate under harsher conditions.

Table 1 Optimization of the Rh NP–rGO catalyzed hydrogenation of quinoline to 1,2,3,4-tetrahydroquinoline in [bmim][BF_4] (note that no other products were observed)[a]

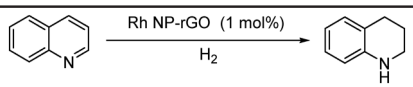

Entry	Pressure (bar)	Time (h)	Yield[b] (%)
1	30	12	>99
2	20	12	98
3	10	12	93
4	1	12	6
5	10	24	>99
6	10	6	75
7	10	4	67
8	10	1	38

[a] Reaction conditions: Rh NP–rGO (1 mol% in [bmim][BF_4]), substrate (1.0 mmol), 80 °C. [b] GC yield.

The substrate scope of the Rh NP–rGO catalyst, obtained by the microwave-assisted method, was explored under mild reaction conditions (Table 2). Quinoline derivatives were converted to their respective 1,2,3,4-tetrahydroquinolines in high yields of up to 87% (Table 2, entries 1–7). Only the reduction of the heteroarene ring was observed. The functional group tolerance of the catalyst was studied using some challenging substrates with various functional groups attached to different parts of the heteroarene structure. The hydrogenation of hydroxyl, aldehyde and amine substituted quinolines using the Rh NP–rGO composite gave the corresponding products in high yields and reduction of the functional group was not observed. Notably, in the presence of an aldehyde group, which is highly reactive towards reduction,[51,52] only the heteroarene ring was hydrogenated (Table 2, entry 5), demonstrating the excellent chemoselectivity of the catalyst. Indeed, the presence of electron donating or withdrawing substituents on the aromatic ring does not affect the selectivity of the reaction.

The hydrogenation of pyridine derivatives, which is important for the chemical and pharmaceutical industries, usually requires harsh reaction conditions.[53] The Rh NP–rGO catalyst is able to hydrogenate pyridine and methyl-substituted pyridines at 80 °C under 10 bar of H_2 affording the corresponding piperidine derivatives in excellent yields (Table 2, entries 8–10). Indole can also be hydrogenated into 1,2,3,4-tetrahydroindole in 72% yield under mild conditions (Table 2, entry 11).

The Rh NP–rGO catalyst was also assessed in the hydrogenation of oxygen containing heterocycles. The reduction of furan to tetrahydrofuran in quantitative yield was achieved at room temperature (Table 3, entry 1). NMR spectroscopy and ESI-MS of the reaction mixture before and after the catalysis indicate that the IL is stable (Fig. S6–S10, ESI†). The Rh NP–rGO catalyst was also evaluated in water and glycerol. The yield remains higher in these solvents for N-heterocyclic substrates (Table S1, ESI†).

The utility of the catalyst was evaluated in the hydrogenation of complex molecules, *i.e.* furanochromone and furanocoumarin derivatives. Visnagin, 8-methoxypsoralen and khellin were efficiently converted under 10 bar of H_2 at 80 °C with the respective products obtained in high yields (Table 3, entries 2–4). Remarkably, only the unsaturated C=C bonds in the two heterocyclic rings in visnagin are reduced affording tetrahydrovisnagin in 94% yield, and the catalyst is completely selective towards the aromatic ring in the hydrogenation of other complex molecules.

Table 2 Evaluation of the substrate scope of the Rh NP–rGO catalyst in [bmim][BF_4][a]

Entry	Substrate	Product	Yield[b] (%)
1			86
2	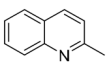	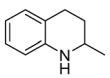	71
3	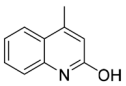	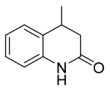	75
4			59[c]
5			87[c]
6	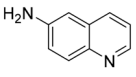	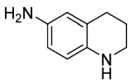	80[c]
7	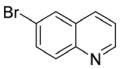	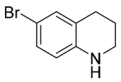	76
8			99[c]
9			78[c]
10			82[c]
11			72[d]

[a] Reaction conditions: Rh NP–rGO (1 mol% in [bmim][BF_4], 2.0 mL), substrate (1.0 mmol), H_2 (10 bar) 80 °C, 15 h. [b] GC yield. [c] 8 h. [d] 70 h.

Table 3 Hydrogenation of oxygen containing heterocycles using the Rh NP–rGO catalyst in [bmim][BF_4][a]

Entry	Substrate	Product	Yield[b] (%)
1			99[c]
2	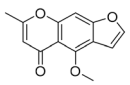 Visnagin	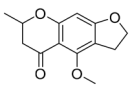	94
3	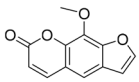 8-Methoxy psoralen	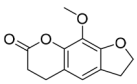	92
4	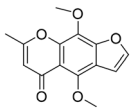 Khellin	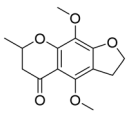	60

[a] Reaction conditions: substrate (1 mmol), Rh NP–rGO (1 mol%), [bmim][BF_4] (2.0 mL), H_2 (10 bar), 80 °C, 36 h. [b] Isolated yield. [c] 25 °C.

The recyclability of the Rh NP–rGO catalyst was studied as catalysts typically used in the hydrogenation of quinolines are often difficult to recycle due to poisoning by reaction intermediates. The reaction time and conditions for the recycling experiments were optimized for the reduction of quinoline over several runs (Fig. 3), with only a slight loss of catalytic activity observed over the five cycles. The loss of activity can be easily compensated, by increasing the reaction time or adding a small amount of fresh catalyst. The selectivity towards the 1,2,3,4-tetrahydroquinoline product remained at 100% throughout the five cycles.

Experimental

Materials and methods

All chemicals were obtained commercially and used without further purification except for [bmim][BF_4], which was dried and deoxygenated under vacuum prior to use. All manipulations with $Rh_6(CO)_{16}$ were carried out under an inert atmosphere in a glovebox or using Schlenk techniques. Microwave synthesis was carried out using a laboratory microwave system CEM Discover. Transmission electron microscopy (TEM) of the composites on a Ted-Pella standard carbon-coated copper grid (methanol was used to disperse the composites) was performed on an FEI Talos F200S electron microscope operating at 300 eV. The obtained micrographs were processed using Fiji software. Surface area analysis was performed with a Micromeritics 3Flex instrument. The samples were outgassed at 3 mTorr and 120 °C (2 °C min^{-1}) for 4 h prior to analysis. The Rh content in the graphene-supported rhodium catalysts was determined by atomic absorption spectroscopy (AAS) using a Shimadzu AA-6650 spectrometer with an air–acetylene flame from the diluted solutions in *aqua regia* (1/3 v/v HNO_3/HCl). The sample (10 mg) was digested in hot *aqua regia* (20 mL, HCl (37%) : HNO_3 (65%) 3 : 1), slowly heated to dryness and the residue was re-dissolved in concentrated HCl

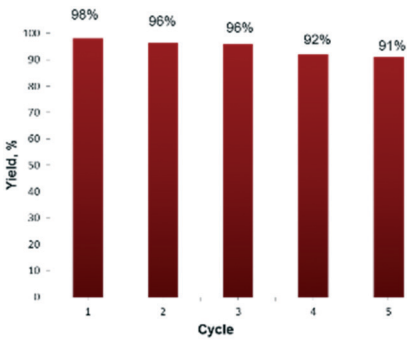

Fig. 3 Recycling of the Rh NP–rGO catalyst in [bmim][BF_4] in the hydrogenation of quinoline to 1,2,3,4-tetrahydroquinoline. Reaction conditions: Rh NP–rGO (30 mg, 0.05 mmol Rh), quinoline (5.0 mmol), [bmim][BF_4] (10.0 mL), H_2 (10 bar), 80 °C, 60 h.

(20 mL, 37%). The solution was filtered, *aqua regia* was added to a total volume of 50 mL and the solution was analyzed by AAS. X-ray photoelectron spectroscopy (XPS) measurements were carried out using a PHI VersaProbe II scanning XPS microprobe (Physical Instruments AG, Germany). Analysis was performed using a monochromatic Al Kα X-ray source of 24.8 W power with a beam size of 100 μm. The spherical capacitor analyser was set at 45° take-off angle with respect to the sample surface. The pass energy was 46.95 eV yielding a full width at half maximum of 0.91 eV for the Ag $3d_{5/2}$ peak. Curve fitting was performed using the PHI Multipak software. Powder X-ray diffraction (XRD) was performed using a PANalytical Empyrean XRD with a Bragg–Brentano geometry fitted with a PANalytical PIXcel-1D detector using Ni filtered Cu-Kα radiation (λ = 1.54056 Å). Data were collected at 45 kV and 40 mA in continuous mode with a scanning rate of 0.01° min^{-1} in the 2θ range between 4 and 94°. The catalytic reactions were performed under H_2 in high pressure Parr autoclaves. Quantitative analysis was performed using a GC/MS Agilent 7000C equipped with a 30 m HP-5 0.5 mm column with a 0.25 μm coating and a flame ionization detector.

rGO was prepared according to reference protocols by transforming graphite into graphite oxide using the Hummers/Offeman[54] process followed by reduction with hydrazine.[34]

Synthesis of the Rh NP–rGO composite *via* thermal decomposition

rGO (9.6 mg, 0.2 wt% based on [bmim][BF_4]) was dispersed in degassed [bmim][BF_4] at room temperature for 20 h with ultrasound treatment during the first 2 h. $Rh_6(CO)_{16}$ (83 mg) was added to the mixture (1 wt% metal, relative to 4.8 g [bmim][BF_4]) and the suspension was stirred for 18 h under a nitrogen atmosphere. The solution was heated to 230 °C for 18 h under stirring. After cooling to room temperature, an aliquot of the mixture was collected for TEM characterization. The slurry was then degassed (to remove any residual carbon monoxide) under vacuum and washed with distilled water (10 mL) to remove the ionic liquid from the Rh NP–rGO composite. The black suspension was centrifuged (2 × 20 min, 10 000 rpm) and the water–ionic liquid phase was decanted. The resulting precipitate was washed with water and separated by centrifugation and decantation three times. Finally, the residue was dispersed in water (10 mL), filtered and dried under vacuum, yielding black-grey flakes corresponding to the Rh NP–rGO composite. The Rh loading in the material was determined by AAS.

Synthesis of the Rh NP–rGO composite *via* microwave dielectric heating

rGO (57.6 mg, 0.2 wt% based on the ionic liquid [bmim][BF_4]) was dispersed in deoxygenated [bmim][BF_4] at room temperature for 20 h with additional ultrasound treatment during the first 2 h. $Rh_6(CO)_{16}$ (249 mg) was added to the mixture (1 wt% metal, relative to 14.4 g [bmim][BF_4]) and stirred for 18 h under a nitrogen atmosphere until a homogeneously dispersed mixture was formed. Then, the mixture was divided into portions of 1.5 mL (due to the configuration of the microwave system) and placed into microwave vials under a nitrogen atmosphere. The mixtures were subjected to microwave irradiation ("fixed power" regime, 20 W, 6 min, maximal temperature 300 °C, "control" mode, no ventilation) under a nitrogen atmosphere, and the irradiation and heating regime were kept constant. After cooling to room temperature, an aliquot of the mixture was collected for TEM characterization. The slurry was then degassed under vacuum and washed with distilled water (30 mL) to remove [bmim][BF_4]. The black suspension was centrifuged (2 × 20 min, 10 000 rpm), the liquid water–ionic liquid phase was decanted and this procedure was repeated three times. Finally, the precipitate was dispersed in water (30 mL), filtered and dried under vacuum, yielding black-grey flakes corresponding to the Rh NP–rGO composite. The Rh loading in the material was determined by AAS.

General procedure for the hydrogenation reactions

An autoclave with a glass inlay was used to conduct the hydrogenation reactions. In a typical reaction, the Rh NP–rGO catalyst (0.01 mmol Rh, 6 mg of the catalyst powder) was placed into the vessel and the substrate (1.0 mmol) and [bmim][BF_4] (2.0 mL) were added. The autoclave was sealed and purged with H_2, pressurized to 10 bar and then heated to 80 °C. After the appropriate time, the heating was stopped, the autoclave cooled to room temperature and the residual gas pressure released. Ethyl acetate (20 mL) was added and the mixture was stirred for 48 h. The ethyl acetate layer was separated and analyzed by GC (using decane as an internal standard). Note that prior to catalytic tests, mass transfer limitations in the system were evaluated using the stirring rate criterion. The quinoline conversion levels achieved at different stirring rates indicated that the conversion was not affected by the stirring rate if the stirring rate was set between 1200 and 1500 rpm. Thus, the stirring rate was maintained at a constant speed of 1500 rpm.

Recycling experiments for the hydrogenation of quinoline

The Rh NP–rGO catalyst (0.05 mmol Rh, 30 mg of the catalyst powder) was placed in an autoclave and quinoline (5.0 mmol) and [bmim][BF_4] (10.0 mL) were added. The autoclave was sealed and purged with H_2, pressurized to 10 bar and then heated to 80 °C. After 60 h, the heating was stopped, the autoclave cooled to room temperature and the residual gas pressure released. Ethyl acetate (100 mL) was added and the mixture was stirred for 48 h. The extraction mixture was separated and the organic layer was analyzed by GC (using decane as an internal standard). The [bmim][BF_4] layer containing the Rh NP–rGO catalyst was collected and any residual volatiles were removed under vacuum. The catalyst was placed in the autoclave and a new portion of quinoline (5.0 mmol) was added to repeat the catalytic procedure.

Conclusions

A rGO supported Rh NP nanocomposite material prepared in [bmim][BF_4] using microwave dielectric heating, termed Rh NP–rGO, is a highly effective catalyst for the selective reduction of heterocyclic rings, *e.g.* quinolines and benzofurans, even in the presence of other reducible functionalities. The microwave-assisted ionic liquid synthesis affords a fine dispersion of Rh NPs on the surface of rGO sheets, which leads to the high activity and recyclability. The catalyst prepared using the microwave treatment is superior to that prepared *via* conventional thermal methods. Moreover, compared to other catalysts used for the selective reduction of heterocyclic substrates, the Rh NP–rGO system is more selective and operates at lower pressures and temperatures. Furthermore, the Rh NP–rGO catalyst could also be recycled several times without a significant loss of selectivity.

Conflicts of interest

There are no conflicts to declare.

Acknowledgements

We thank the Swiss National Science Foundation and EPFL for financial support. We are also grateful to CIME (Interdisciplinary Centre for Electron Microscopy, EPFL) and Dr. Thomas LaGrange for the assistance with the characterization of the NPs. We thank Dr. Pierre Mettraux for the assistance with XPS measurements and Dr. Arnaud Magrez for the assistance with XRD analysis.

References

1 M. Freifelder, *Adv. Catal.*, 1963, **14**, 203–253.
2 D.-S. Wang, Q.-A. Chen, S.-M. Lu and Y.-G. Zhou, *Chem. Rev.*, 2012, **112**, 2557–2590.
3 C. Deraedt, R. Ye, W. T. Ralston, F. D. Toste and G. A. Somorjai, *J. Am. Chem. Soc.*, 2017, **139**, 18084–18092.
4 D. Ren, L. He, L. Yu, R.-S. Ding, Y.-M. Liu, Y. Cao, H.-Y. He and K.-N. Fan, *J. Am. Chem. Soc.*, 2012, **134**, 17592–17598.
5 A. Sánchez, M. Fang, A. Ahmed and R. A. Sánchez-Delgado, *Appl. Catal., A*, 2014, **477**, 117–124.
6 M. Guo, C. Li and Q. Yang, *Catal. Sci. Technol.*, 2017, **7**, 2221–2227.
7 L. Tao, Q. Zhang, S.-S. Li, X. Liu, Y.-M. Liu and Y. Cao, *Adv. Synth. Catal.*, 2015, **357**, 753–760.
8 Y. Gong, P. Zhang, X. Xu, Y. Li, H. Li and Y. Wang, *J. Catal.*, 2013, **297**, 272–280.
9 Q.-L. Zhu and Q. Xu, *Chem*, 2016, **1**, 220–245.
10 J. Pyun, *Angew. Chem., Int. Ed.*, 2011, **50**, 46–48.
11 P. P. Upare, M. Lee, S.-K. Lee, J. W. Yoon, J. Bae, D. W. Hwang, U. H. Lee, J. S. Chang and Y. K. Hwang, *Catal. Today*, 2016, **265**, 174–183.
12 C. Huang, C. Li and G. Shi, *Energy Environ. Sci.*, 2012, **5**, 8848–8868.
13 G. Goncalves, P. A. A. P. Marques, C. M. Granadeiro, H. I. S. Nogueira, M. K. Singh and J. Grácio, *Chem. Mater.*, 2009, **21**, 4796–4802.
14 S. Basu and S. K. Hazra, *C*, 2017, **3**, 29.
15 A. V. Singhal, H. Charaya and I. Lahiri, *Crit. Rev. Solid State Mater. Sci.*, 2017, **42**, 499–526.
16 A. C. H. Tsang, H. Y. H. Kwok and D. Y. C. Leung, *Solid State Sci.*, 2017, **67**, A1–A14.
17 D. Wang, R. Zhang, J. Li, X. Hao, C. Ding, L. Zhao, G. Wen, J. Liu and W. Zhou, *J. Mater. Chem. A*, 2017, **5**, 1687–1697.
18 R. Bajpai, S. Roy, P. Kumar, P. Bajpai, N. Kulshrestha, J. Rafiee, N. Koratkar and D. S. Misra, *ACS Appl. Mater. Interfaces*, 2011, **3**, 3884–3889.
19 G. Lee, J. H. Shim, H. Kang, K. M. Nam, H. Song and J. T. Park, *Chem. Commun.*, 2009, 5036–5038.
20 R. Nie, J. Wang, L. Wang, Y. Qin, P. Chen and Z. Hou, *Carbon*, 2012, **50**, 586–596.
21 D. Wang, W. Niu, M. Tan, M. Wu, X. Zheng, Y. Liu and N. Tsubaki, *ChemSusChem*, 2014, **7**, 1398–1406.
22 F. Chen, A.-E. Surkus, L. He, M.-M. Pohl, J. Radnik, C. Topf, K. Junge and M. Beller, *J. Am. Chem. Soc.*, 2015, **137**, 11718–11724.
23 X. Cui, Y. Li, S. Bachmann, M. Scalone, A.-E. Surkus, K. Junge, C. Topf and M. Beller, *J. Am. Chem. Soc.*, 2015, **137**, 10652–10658.
24 M. Tan, G. Yang, T. Wang, T. Vitidsant, J. Li, Q. Wei, P. Ai, M. Wu, J. Zheng and N. Tsubaki, *Catal. Sci. Technol.*, 2016, **6**, 1162–1172.
25 K. Schütte, J. Barthel, M. Endres, M. Siebels, B. M. Smarsly, J. Yue and C. Janiak, *ChemistryOpen*, 2017, **6**, 137–148.
26 S. Wegner and C. Janiak, *Top. Curr. Chem.*, 2017, **375**, 65.
27 C. Daguenet, P. J. Dyson, I. Krossing, A. Oleinikova, J. Slattery, C. Wakai and H. Weingärtner, *J. Phys. Chem. B*, 2006, **110**, 12682–12688.
28 H. Weingärtner, P. Sasisanker, C. Daguenet, P. J. Dyson, I. Krossing, J. M. Slattery and T. Schubert, *J. Phys. Chem. B*, 2007, **111**, 4775–4780.
29 D. D. Lovingood and G. F. Strouse, *Nano Lett.*, 2008, **8**, 3394–3397.
30 C. Vollmer, E. Redel, K. Abu-Shandi, R. Thomann, H. Manyar, C. Hardacre and C. Janiak, *Chem. – Eur. J.*, 2010, **16**, 3849–3858.
31 D. Marquardt, C. Vollmer, R. Thomann, P. Steurer, R. Mülhaupt, E. Redel and C. Janiak, *Carbon*, 2011, **49**, 1326–1332.
32 M.-G. Ma, Y.-Y. Dong, L.-H. Fu, S.-M. Li and R.-C. Sun, *Carbohydr. Polym.*, 2013, **15**, 1669–1676.
33 M.-G. Ma, J.-F. Zhu, Y.-J. Zhu and R.-C. Sun, *Chem. – Asian J.*, 2014, **9**, 2378–2391.
34 H. Yang, C. Shan, F. Li, D. Han, Q. Zhang and L. Niu, *Chem. Commun.*, 2009, 3880–3882.
35 M. S. L. Hudson, H. Raghubanshi, S. Awasthi, T. Sadhasivam, A. Bhatnager, S. Simizu, S. G. Sankar and O. N. Srivastava, *Int. J. Hydrogen Energy*, 2014, **39**, 8311–8320.
36 Z. Bo, X. Shuai, S. Mao, H. Yang, J. Qian, J. Chen, J. Yan and K. Cen, *Sci. Rep.*, 2014, **4**, 4684.
37 M. Thommes, *Chem. Ing. Tech.*, 2010, **82**, 1059–1073.

38 J. F. Moulder, *Handbook of X-ray Photoelectron Spectroscopy: A Reference Book of Standard Spectra for Identification and Interpretation of XPS Data*, Physical Electronics Division, Perkin-Elmer Corporation, 1992.
39 J.-Y. Lee and L.-K. Liu, *Int. J. Hydrogen Energy*, 2014, **39**, 17492–17500.
40 N. Dahal, S. García, J. Zhou and S. M. Humphrey, *ACS Nano*, 2012, **6**, 9433–9446.
41 S. M. Choi, M. H. Seo, H. J. Kim and W. B. Kim, *Synth. Met.*, 2011, **161**, 2405–2411.
42 Y. Wang, Z. Song, D. Ma, H. Luo, D. Liang and X. Bao, *J. Mol. Catal. A: Chem.*, 1999, **149**, 51–61.
43 J. Shen, L. Yang, K. Hu, W. Luo and G. Cheng, *Int. J. Hydrogen Energy*, 2015, **40**, 1062–1070.
44 A. B. Kroner, M. A. Newton, M. Tromp, A. E. Russell, A. J. Dent and J. Evans, *ChemPhysChem*, 2013, **14**, 3606–3617.
45 H.-Y. Jiang and X.-X. Zheng, *Appl. Catal., A*, 2015, **499**, 118–123.
46 Z.-P. Zhang, W. Zhu, C.-H. Yan and Y.-W. Zhang, *Chem. Commun.*, 2015, **51**, 3997–4000.
47 A. Gniewek and A. M. Trzeciak, *Top. Catal.*, 2013, **56**, 1239–1245.
48 S. Caporali, U. Bardi and A. Lavacchi, *J. Electron Spectrosc. Relat. Phenom.*, 2006, **151**, 4–8.
49 L. Luza, C. P. Rambor, A. Gual, J. A. Fernandes, D. Eberhardt and J. DuPont, *ACS Catal.*, 2017, **7**, 2791–2799.
50 A. Karakulina, A. Gopakumar, I. Akcok, B. L. Roulier, T. LaGrange, S. A. Katsyuba, S. Das and P. J. Dyson, *Angew. Chem., Int. Ed.*, 2016, **55**, 292–296.
51 S. Das, D. Addis, S. Zhou, K. Junge and M. Beller, *J. Am. Chem. Soc.*, 2010, **132**, 1770–1771.
52 D. Goncalez-Galvez, P. Iara, O. Rivada-Wheeloghan, S. Conejero, B. Chaudret, K. Philippot and P. W. N. M. van Leeuwen, *Catal. Sci. Technol.*, 2013, **3**, 99–105.
53 M. Freifelder, *Catalytic Hydrogenation in Organic Synthesis – Procedures and Commentary*, Wiley-Interscience, New York, 1978.
54 W. S. Hummers Jr. and R. E. Offeman, *J. Am. Chem. Soc.*, 1958, **80**, 1339–1339.